COMPARISON OF 1-D AND 2-D SURFACE COIL ARRAYS FOR ACCELERATED VOLUME MR IMAGING USING SENSITIVITY ENCODING

Peter Kellman[1], Martin J. Schnermann[2], Elliot R. McVeigh[1]

[1]National Institutes of Health, National Heart, Lung, and Blood Institute, Bethesda, MD, USA
[2]Colby College, Waterville, ME, USA

ABSTRACT

The sensitivity encoding (SENSE) [1] method of parallel MR accelerated imaging is evaluated and compared for 1-d and 2-d surface coil array geometries. Accelerated MR imaging using SENSE may be applied to volume imaging using either 3-d or 2-d multi-slice acquisition strategies. For higher accelerations such as rate R=4, 3-d SENSE may be applied along either or both phase encode directions. Image quality (SENSE g-factor) is compared for R=4 acceleration implemented with a reduced number of phase encodes in the y-direction, and (assuming a 3-d acquisition) with a reduced number of phase encodes in both y- and z-directions. Simulations show that the performance for 1-d and 2-d array geometries depends highly on the slice orientation.

1. INTRODUCTION

Parallel imaging methods for accelerated MR imaging are becoming practical due to the increased affordability of multi-channel digital receiver systems. The sensitivity encoding (SENSE) [1] method of parallel imaging incurs a loss in SNR due to both reduced imaging time and sub-optimal coil geometry (the so called g-factor). The g-factor represents the inflation in variance due to the ill-conditioning of the SENSE inverse solution, which depends on the acceleration rate, the number of coils, specific coil sensitivity profiles, and slice geometry. Therefore, it is of interest to investigate the dependence of g-factor on various coil geometries. Previous studies have been reported which optimize linear coil arrays for SENSE application [2,3]. In this study, we investigate the dependence of g-factor for both 1-d (linear) and 2-d (area) arrays for various slice geometries. We also compare the g-factor performance for 3-d volume imaging using acceleration along two phase encode directions versus acceleration along a single phase encode direction (this latter case may use 2d or 3d imaging). These results are also applicable to volume imaging using SENSE for separation of multiple slices simultaneously excited [4].

The optimum phased array combined SNR (B1-weighted) [5] and SENSE g-factor were computed for various coil geometries and imaging plane orientations based on simulated field maps. Magnetic fields (B1-maps) for each coil were calculated using the Biot-Savart law. The sample noise correlations between coils which are used in calculating the optimum B1-weighted combining and SENSE g-factor [1] were calculated from the magnetic vector potential (A-field).

2. METHODS

2.1. Coil Geometry

The body was modeled as an elliptical cylinder with uniform conductivity as depicted in Figure 1 with multiple axial image planes overlaid. Surface coils arrays were composed of rectangular coil elements which were tangent to the elliptical surface at the center of each coil. The tangent was spaced by a gap of 1 cm from the body. Results are presented comparing the performance between a 1-d linear array configuration (Fig. 2(a)) and a 2-d array configuration (Fig. 2(b)). The dimensions which correspond to the results are: 206 mm short axis x 326 mm long axis body ellipse, 10 mm coil standoff, 45x210 mm^2 elements for linear arrays, and 100x100 mm^2 elements for 2x2 arrays. The spacing between adjacent coil elements was varied. The results provided are for a 10 mm gap between elements. A 160 mm thick slab was imaged with 32 slices spaced 5 mm.

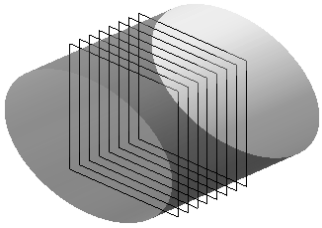

Figure 1. Geometry of elliptical cylinder and axial imaging planes.

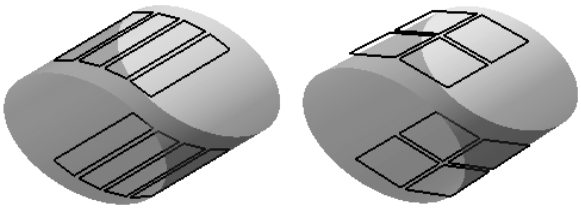

(a) (b)

Figure 2. Geometry of surface coil array configurations (a) 1-d linear array and (b) 2-d 2x2 array.

2.2. SENSE SNR and G-factor Calculation

The SENSE [1] technique exploits the differences in spatial sensitivity of multiple receiver coils to eliminate the aliased component that results from undersampling *k*-space. The formulation of *R*=4 sensitivity encoding (SENSE) is presented for the case of 3-d imaging using Cartesian *k*-space sampling. Consider 2 cases for undersampling. In the first case, consider undersampling along a single phase encode direction, *y*. In this case, the received signals may be written as:

$$\begin{bmatrix} g_1(x,y,z) \\ \vdots \\ g_N(x,y,z) \end{bmatrix} = \begin{bmatrix} s_1(x,y,z) & s_1(x,y-D_y,z) & s_1(x,y-2D_y,z) & s_1(x,y-3D_y,z) \\ \vdots & & & \vdots \\ s_N(x,y,z) & s_N(x,y-D_y,z) & s_N(x,y-2D_y,z) & s_N(x,y-3D_y,z) \end{bmatrix} \begin{bmatrix} f(x,y,z) \\ f(x,y-D_y,z) \\ f(x,y-2D_y,z) \\ f(x,y-3D_y,z) \end{bmatrix} + \begin{bmatrix} n_1(x,y,z) \\ \vdots \\ n_N(x,y,z) \end{bmatrix} \quad [1]$$

where $f(x, y, z)$ represents the desired image, $g_i(x,y,z)$ is the reconstructed image for the *i*-th coil, $s_i(x,y,z)$ is the complex sensitivity profile for the *i*-th coil, *N* denotes the number of coils, $D_y=FOV_y/4$ is the distance between ghosts, and n_i is the noise for the *i*-th coil. In the second case, consider undersampling by R=2 along both the y and z phase encode directions for an overall R=4 acceleration. In this case the aliased images for each coil may be written as:

$$\begin{bmatrix} g_1(x,y,z) \\ \vdots \\ g_N(x,y,z) \end{bmatrix} = \begin{bmatrix} s_1(x,y,z) & s_1(x,y-D_y,z) & s_1(x,y,z-D_z) & s_1(x,y-D_y,z-D_z) \\ \vdots & & & \vdots \\ s_N(x,y,z) & s_N(x,y-D_y,z) & s_N(x,y,z-D_z) & s_N(x,y-D_y,z-D_z) \end{bmatrix} \begin{bmatrix} f(x,y,z) \\ f(x,y-D_y,z) \\ f(x,y,z-D_z) \\ f(x,y-D_y,z-D_z) \end{bmatrix} + \begin{bmatrix} n_1(x,y,z) \\ \vdots \\ n_N(x,y,z) \end{bmatrix} \quad [2]$$

where $D_y=FOV_y/2$ and $D_z=FOV_z/2$. Equations [1] and [2] may be written more compactly as:

$$\mathbf{g}(x,y,z) = \mathbf{S}(x,y,z)\ \mathbf{f}(x,y,z) + \mathbf{n}(x,y,z) \ . \quad [3]$$

In both cases, the desired unaliased full field-of-view images $f(x,y,z)$ may be estimated from the measured aliased images $g_i(x,y,z)$, provided that N≥4 and assuming the coil sensitivities are known or estimated with sufficient accuracy. The generalized weighted least squares solution [1] is given by:

$$\mathbf{f_{SENSE}} = (\mathbf{S^H\ R_n^{-1}\ S})^{-1}\ \mathbf{S^H\ R_n^{-1}\ g} \ , \quad [4]$$

where **g** denotes the *N*x1 vector of aliased images (for each coil), $\mathbf{f_{SENSE}}$ denotes the 4x1 vector estimate of unaliased images, **S** is the estimated sensitivity matrix, $\mathbf{R_n}$ is the estimated noise correlation matrix between coils, and superscript ^{H} is the Hermitian operator (conjugate transpose).

The SNR accelerated imaging using the SENSE method may be calculated as:

$$SNR_{SENSE} = SNR_{optimum} \big/ g\sqrt{R} \ , \quad [5]$$

where R is the acceleration factor, $SNR_{optimum}$ is the B1-weighted optimum phased array combining [5] calculated as:

$$SNR_{optimum} = \sqrt{(\mathbf{S}^H\mathbf{R}_n^{-1}\mathbf{S})} \ , \quad [6]$$

and the loss in SNR due to variance inflation, SENSE g-factor [1], is defined as:

$$g(x,y,z) = \frac{1}{\sqrt{(\mathbf{S}^H\mathbf{R}_n^{-1}\mathbf{S})^{-1}_{(k,k)}(\mathbf{S}^H\mathbf{R}_n^{-1}\mathbf{S})_{(k,k)}}} \ , \quad [7]$$

where the subscript *(k,k)* denotes the index of the matrix corresponding to the *k*-th sub-image.

The greatest variation in the overall SENSE SNR (Eq. [5]) for the central ROI is due to the g-factor. The g-factor depends strongly on position (x,y,z) and has several hotspots. Therefore, the performance criteria included both the worst case (maximum) as well as the mean g-factor in the region of interest (ROI). The phase encode direction was chosen as the direction of minimum FOV with FOV equal to the short axis of the ellipse.

For 3-d imaging, the slab profile attenuates the first and last slice to avoid aliasing in the z-direction. In calculating the g-factor for 3-d SENSE, the first and last slice have been zeroed.

2.3. Field Calculations

The magnetic vector potential (A-field) and flux density (B-field) vectors were calculated using the Biot-Savart law evaluated for straight wire segments [6]. Each surface coil was modeled as a set of line segments and the field for each segment was calculated over a 3-dimensional

mesh grid. The A- and B-fields at point P for a line segment defined in Figure 3 (between points P1 and P2 along the z-axis) may be written as:

$$A_Z = \ln\left(\frac{\left(z_2+\sqrt{z_2^{\,2}+x_p^{\,2}+y_p^{\,2}}\right)}{\left(z_1+\sqrt{z_1^{\,2}+x_p^{\,2}+y_p^{\,2}}\right)}\right) \qquad [8]$$

$$\mathbf{B} = \frac{\left(\sin\theta_2-\sin\theta_1\right)}{\sqrt{x_p^{\,2}+y_p^{\,2}}}\begin{bmatrix}-\sin\varphi\\ \cos\varphi\\ 0\end{bmatrix}$$

Linear transformations were applied to calculate the fields for each side (wire segment) of the rectangular coil elements for each grid point in the volume. The complex coils sensitivities for MR imaging, $s_i(x,y,z)$ for coil i (also referred to as B1-map), were then calculated from the tangential B-field components, i.e., $B_x + j\ B_y$, with j defined as √-1 and the main magnetic field (B0) along the z-direction.

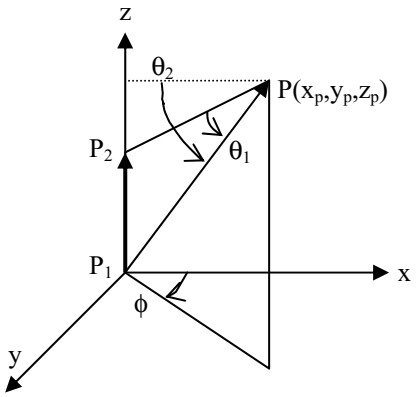

Figure 3. Geometry for calculating field for wire segment.

The noise correlation matrix for sample noise dominated reception was calculated from the A-fields by integration over the volume [5],

$$\mathbf{R}_n(i,j) = \sum_{x,y,z} A_i(x,y,z) \bullet A_j(x,y,z)\ , \qquad [9]$$

where *i,j* indices correspond to coils. The integration was performed over all (x,y) in the elliptical cross-section, and was truncated at a height (z) of 500 mm. With a stand-off distance of 10 mm, it was empirically determined that a grid size of 64x64x64 provided sufficient accuracy.

All calculations were performed using MATLAB (The Mathworks, Natick, MA, USA).

3. RESULTS

The spatially varying g-factor has hotspots in regions where the inverse solution (Eq. [4]) is ill-conditioned. Examples of the g-factor for axial imaging planes are shown in Figure 4 for illustrative purposes. The g-factor for the linear array of Fig. 2(a) is shown in Fig. 4(a) for SENSE applied along the y (R_y=4). The g-factor for the 2x2 array of Fig. 2(b) is shown in Fig. 4(b) for SENSE applied along the y (R_y=4), and in Fig. 4(c) for SENSE applied along the y and z (R_y=R_z=2). These g-factors correspond to a central slice (15 of 32), which represents a worst case geometry for the R_y=R_z=2 SENSE cases of Fig. 4(c). Best cases for R_y=R_z=2 SENSE are at slices 8 and 24. The maximum g-factor is less slice dependent for R_y=4 cases. The g-factor images are scaled with minimum value of 1 and maximum values of 4, 4, and 1.5, for Figures 4(a)-(c), respectively. The elliptical borders are clearly evident as aliased regions in the y-dimension in the g-factor images of Fig. 4, while the aliasing in the z-direction for Fig. 4 (c) is not evident since there is no defined structure in the z-direction for this axial image.

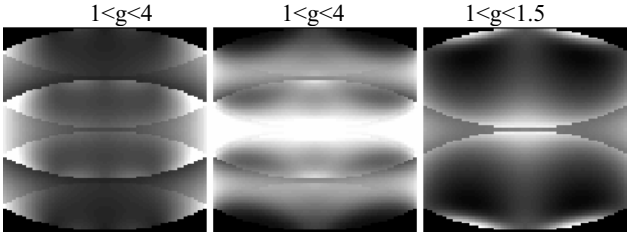

(a) linear array R_y=4 (b) 2x2 array R_y=4 (c) 2x2 array R_y=R_z=2

Figure 4. G-factor images for slice center axial slice.

Values of the maximum and mean g-factor values over the ROI are listed in Tables 1 and 2, respectively, for the various coils and SENSE cases. A circular ROI with diameter of 102 mm (50% of body short axis) was used. The oblique angles were 45º singly oblique about the x-axis, singly oblique about the y-axis, and doubly oblique.

Table 1. Maximum SENSE g-factors in ROI.

	linear array		2x2 array	
	R_y=4	R_y=R_z=2	R_y=4	R_y=R_z=2
axial	2.3	>>10	4.6	1.5
45º singly oblique (x)	1.5	1.5	3.5	1.5
45º singly oblique (y)	2.3	1.7	4.9	1.8
45º doubly oblique	2.0	1.4	4.1	1.8

Table 2. Mean SENSE g-factors in ROI.

	linear array		2x2 array	
	R_y=4	R_y=R_z=2	R_y=4	R_y=R_z=2
axial	2.0	>>10	3.4	1.3
45º singly oblique (x)	1.2	1.3	1.8	1.2
45º singly oblique (y)	1.9	1.4	3.5	1.3
45º doubly oblique	1.7	1.2	2.4	1.2

The maximum g-factor versus the (doubly) oblique angle of the imaging plane is shown in Figure 5 for the linear surface coil array.

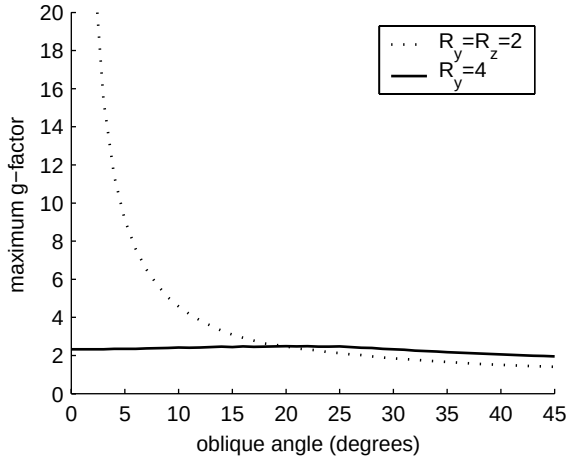

Figure 5. Worst case g-factor in ROI versus oblique angle for linear surface coil array.

4. DISCUSSION

For volume imaging of a slab with axial orientation, 3-d SENSE imaging (R_y=R_z=2) with a 2-d surface coil array has better performance, i.e. lower maximum value of g-factor, than with a linear array (aligned with the axial plane) using either 3-d or 2-d multi-slice imaging. However, as the imaging planes become oblique (array orientation relative to image plane), the g-factor (R_y=R_z=2) improves dramatically for the linear array. For doubly oblique angles of approximately 20º, the linear array performance (mean and max) is comparable to the 2-d array for SENSE both using R_y=R_z=2. The R_y=4 performance of the linear array is significantly better than for 2-d array for all imaging angles tested. In the case of R_y=4, SENSE may be implemented with either 3-d imaging or 2-d multi-slice, making the linear array more versatile on the whole. For oblique angles, the conditioning of the S matrix for the case of 3-d SENSE with R_y=R_z=2 vastly improves since the pixels from the first slice are aliased onto pixels in the center slice that are effectively weighted by the adjacent coil(s). This reduces the collinearity condition (between row vectors of **S**) and thus decreases the g-factor. Furthermore, for fixed coil dimensions, the g-factor for 3d imaging with acceleration along the z worsens as the slab thickness decreases, making the linear array using acceleration along a single (y) phase encode direction more advantageous.

The comparison of worst case g-factors depend heavily on the choice of the ROI since the location of the hotspots for Cartesian SENSE varies with the imaging angle. The ROI diameter was chosen large enough so that this effect was secondary.

5. CONCLUSION

The SENSE g-factor was compared for both linear and 2-d surface coil arrays for R=4 acceleration implemented by 1) reducing the number of phase encodes in the y-direction, and 2) reducing the number of phase encodes in both y- and z-directions (assuming a 3-d acquisition). Simulations show that the performance for 1-d and 2-d array geometries depends highly on the slice orientation. For axial 3-d imaging, the performance of SENSE with the 2-d arrays was better than for 1-d arrays assuming acceleration in both phase encode directions. However, as the imaging plane was sufficiently oblique, linear arrays with acceleration along the y or both y and z phase encode directions performed as well or better.

6. REFERENCES

[1] K.P. Pruessmann, M. Weiger, M.B. Scheidegger, P. Boesiger, “SENSE: sensitivity encoding for fast MRI,” *Magnetic Resonance in Medicine,* Vol. 42(5), pp. 952–962, 1999.

[2] M. Weiger, K.P. Pruessmann, C. Leussler, P. Roschmann, P. Boesiger, “Specific coil design for SENSE: a six-element cardiac array,” *Magnetic Resonance in Medicine*, Vol. 45(3), pp. 495-504, 2001.

[3] J.A. deZwart, P. Ledden, P. van Gelderen, P. Kellman, J.H. Duyn, “Design of a Sensitivity Optimized SENSE MRI Receive Coil for Brain Imaging,” *International Society for Magnetic Resonance in Medicine* Workshop on Minimum MR Data Acquisition Methods. Marco Island, Florida Oct. 2001.

[4] D.J. Larkman, J.V. Hajnal, A.H. Herlihy, G.A. Coutts, I.R. Young, G. Ehnholm, “Use of Multicoil Arrays for Separation of Signal from Multiple Slices Simultaneously Excited,” *Journal of Magnetic Resonance Imaging*, Vol. 13, pp.313-317, 2001.

[5] P.B. Roemer, W.A. Edelstein, C.E. Hayes, S.P. Souza, O.M. Mueller, “The NMR phased array,” *Magnetic Resonance in Medicine,* Vol. 16(2), pp. 192-225. 1990.

[6] M.H. Nayfeh, M.K. Brussel, “Electricity and Magnetism,” Wiley, NewYork, 1985, pp. 244-267.